Investigation of Reaction Mechanisms of Drug Degradation in the Solid State: A Kinetic Study Implementing Ultrahigh–Performance Liquid Chromatography and High–Resolution Mass Spect…

6 AUTHORS, INCLUDING:

Chris Bielow

Max-Delbrück-Centrum für Molekulare Medizin

16 PUBLICATIONS **177** CITATIONS

SEE PROFILE

Reinert Knut

Freie Universität Berlin

142 PUBLICATIONS **21,052** CITATIONS

SEE PROFILE

Hermann Stuppner

University of Innsbruck

354 PUBLICATIONS **4,664** CITATIONS

SEE PROFILE

Christian G Huber

University of Salzburg

191 PUBLICATIONS **4,998** CITATIONS

SEE PROFILE

Investigation of Reaction Mechanisms of Drug Degradation in the Solid State: A Kinetic Study Implementing Ultrahigh-Performance Liquid Chromatography and High-Resolution Mass Spectrometry for Thermally Stressed Thyroxine

Volker Neu,[†] Chris Bielow,[‡] Peter Schneider,[§] Knut Reinert,[‡] Hermann Stuppner,[§] and Christian G. Huber*,[†]

[†]Department of Molecular Biology, Division of Chemistry and Bioanalytics, University of Salzburg, Hellbrunner Strasse 34, 5020 Salzburg, Austria

[‡]Department for Computer Science and Mathematics, Algorithmic Bioinformatics, Free University of Berlin, Takustrasse 9, 14195 Berlin, Germany

[§]Institute of Pharmacy, Pharmacognosy, Member of CMBI, University of Innsbruck, Innrain 80-82, 6020 Innsbruck, Austria

S *Supporting Information*

ABSTRACT: A reaction scheme was derived for the thermal degradation of thyroxine in the solid state, using data obtained from ultrahigh-performance liquid chromatography and high-resolution mass spectrometry (UHPLC-HRMS). To study the reaction mechanism and kinetics of the thermal degradation of the pharmaceutical in the solid state, a workflow was developed by generating compound-specific, time-dependent degradation or formation curves of at least 13 different degradation products. Such curves allowed one to distinguish between first- and second-generation degradation products, as well as impurities resulting from chemical synthesis. The structures of the degradation products were derived from accurate molecular masses and multistage mass spectrometry. Deiodination and oxidative side chain degradation were found to be the major degradation reactions, resulting in the formation of deiodinated thyroxines, as well as acetic acid, benzoic acid, formaldehyde, acetamide, hydroxyacetic acid, oxoacetic acid, hydroxyacetamide, or oxoacetamide derivatives of thyroxine or deiodinated thyroxine. Upon additional structural verification of mass spectrometric data using nuclear magnetic resonance spectroscopy, this comprehensive body of data sheds light on an elaborate, radical-driven reaction scheme, explaining the presence or formation of impurities in thermally stressed thyroxine.
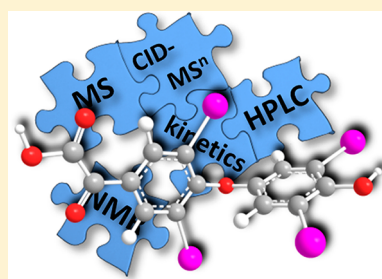
egulations of the U.S. Food and Drug Administration (FDA) and the European Medicines Agency (EMEA) require full proof that drugs admitted to the market are consistent with safety and efficacy.[1] This also mandates that the stability and degradation of drug compounds under conditions of production and storage are well-studied and well-documented. Thyroid hormones such as thyroxine (levothyroxine) and triiodothyronine (liothyronine) play central roles in the human body.[2,3] Worldwide, up to 1 billion people show a deficiency of thyroid hormones, which is normally treated by substitution or supplemental therapy with synthetic hormone.[4] Thyroxine was first isolated from the thyroid gland in 1919[5] and first synthetically prepared in 1927.[6] Today, the pharmaceutical compound is usually synthesized by proprietary multistep chemical synthesis.[7,8] Because byproducts and degradation products of synthetic levothyroxine have been shown to mediate physiological effects, extensive control of the synthetic drug and its impurities is mandatory.[9–11] In this respect, degradation of the drug as bulk material, especially in the solid state, becomes highly important.

The kinetics of degradation showed that deiodination remains the main decomposition reaction of thyroxine under aqueous acidic or alkaline conditions.[12] In the same study, thermal treatment of the solid compound was postulated to generate a cinnamic acid derivative upon deamination and, finally, a benzaldehyde derivative upon oxidative decarboxylation of the amino acid, while no deiodination products were referred. A more-detailed study of liothyronine degradation employing high-performance liquid chromatography-low-resolution quadrupole mass spectrometry revealed 12 different thermal degradation products, including deiodinated derivatives as well as acetic acid-, acetamide-, ethyl- and ethyl alcohol-related derivatives.[9]

With the introduction of ultrahigh-performance liquid chromatography (UHPLC),[13] very rapid and high-resolution separations of pharmaceutical compounds became feasible, facilitating high productivity and cost efficiency in pharmaceut-

ical analysis. Similarly, high-resolution mass spectrometry (HRMS) that employs novel mass analyzers such as the Orbitrap,[14] makes mass determinations with accuracies in the sub-ppm range attainable, enabling a much more efficient identification and structural elucidation of the compounds separated by UHPLC.

In this work, for the first time, we address the challenging field of analyzing the reaction mechanism of thermal degradation in the solid state by comparative UHPLC-HRMS analysis of differentially stressed samples using substance-specific degradation curves. The presented workflow provides an interesting alternative to other techniques applied for impurity profiling such as high-performance liquid chromatography solid-phase extraction—nuclear magnetic resonance (NMR) spectroscopy and gas chromatography—mass spectrometry using dissolved samples, or solid-state NMR spectroscopy, infrared spectroscopy, and powder diffractometry for direct analysis in solid phase,[15−17] since it allows comprehensive insights into considerably complex impurity patterns at very short analysis times.

■ EXPERIMENTAL SECTION

Chemicals and Samples. Eluents were prepared from deionized water (prepared by a Milli-Q system, Millipore, Billerica, MA, USA), acetonitrile (optigrade, from Promochem, Wesel, Germany), and formic acid (purissimum, from Sigma–Aldrich, Steinheim, Germany). Synthetic thyroid hormone samples, including thyroxine as well as 4-(4-hydroxyphenyl)-3,5-diiodo-L-tyrosine (diodothyronine), 4-(4-hydroxy-3-iodophenyl)-3-iodo-L-tyrosine (reverse diiodothyronine), 4-(4-hydroxy-3-iodophenyl)-3,5-diiodo-L-tyrosine (triiodothyronine or liothyronine), 4-(4-hydroxy-3,5-diiodophenyl)-3-iodo-L-tyrosine (reverse triiodothyronine), 4-(4-hydroxyphenoxy)-3,5-diiodophenylacetic acid (diiodothyroacetic acid), 4-(4-hydroxy-3-iodophenoxy)-3,5-diiodophenylacetic acid (triiodothyroacetic acid), 4-(4-hydroxy-3-iodophenoxy)-3,5-diiodophenylpropionic acid (triiodothyropropionic acid), 4-(4-hydroxy-3,5-diiodophenoxy)-3,5-diiodophenylacetic acid (tetraiodothyroacetic acid), and 4-(4-hydroxy-3,5-diiodophenoxy)-3,5-diiodophenylbenzoic acid (tetraiodothyrobenzoic acid) were kindly provided by Peptido GmbH (Bexbach, Germany). The corresponding structures are shown in Figure S-1 of the Supporting Information. In order to simplify the nomenclature of thyroxine derivatives, the recurring structural element specified by "4-(4-hydroxy-3,5-diiodophenoxy)-3,5-diiodophenyl" will be named as "tetraiodothyro". Derivatives containing less than four I atoms contain the analogous structural element "triiodothyo-" or "diiodothyo". Two different stressing conditions were employed, including keeping the compound in an oven for 6 months at 40 °C and finally for 16 h at 60 °C (protocol 1) or keeping it for 48 h at 100 °C (protocol 2). The hormones were dissolved in methanol (LC-MS Chromasolv from Fluka, Buchs, Switzerland)—water solution (50:50) containing 400 mg L^{-1} sodium hydroxide (Merck, Darmstadt, Germany).

Ultrahigh-Performace Liquid Chromatography–High-Resolution Mass Spectrometry (UHPLC-HRMS). Thyroid hormone separations were performed using a 100 mm × 2.1 mm i.d. Hypersil Gold column (Thermo Fisher Scientific, Bremen, Germany) packed with 1.9-µm octadecyl silica particles and an Accela UHPLC system controlled by XCalibur LC-Devices 2.01 software capable of operation up to 1000 bar from Thermo Fisher Scientific. Chromatographic conditions are given in the legend of Figure 1. Data was evaluated with the
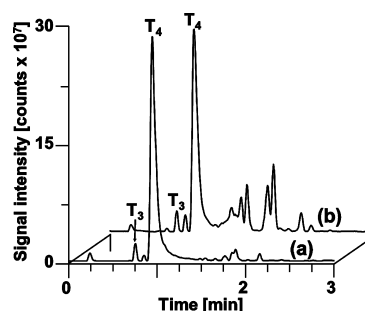

Figure 1. Comparison of UHPLC-HRMS base-peak chromatograms of (a) unstressed and (b) thermally stressed thyroxine. Column, 1.9 µm Hypersil GOLD, 100 mm × 2.1 mm i.d.; sample, 6 µL of 2000 ppm thyroxine solution; gradient: 30%−80% acetonitrile in 0.10% formic acid in 2.1 min, 0.3 min at 80% acetonitrile; flow rate: 1000 µL/min; 60 °C; full scan LTQ-Orbitrap MS detection with m/z = 200−2000.

XCalibur V2.0.7 software from Thermo Fisher Scientific. Mass spectra were recorded on a linear ion trap−Orbitrap instrument (Model LTQ-Orbitrap XL from ThermoFisher Scientific) equipped with the Ionmax electrospray ionization source.

Semipreparative Fractionation and Nuclear Magnetic Resonance Spectroscopy. Semipreparative fractionations of each 20-mg stressed sample dissolved in 2 mL of methanol/water/sodium hydroxide were performed with a 150 mm × 10 mm i.d. Synergy Polar-RP column from Phenomenex (Aschaffenburg, Germany) packed with 4-µm particles, and an analytical HPLC system (Model 1050, Agilent Technologies, Waldbronn, Germany). The gradient was 30% acetonitrile in 0.10% formic acid for 5.0 min, followed by 30%−70% acetonitrile in 0.10% formic acid in 37 min and 80% acetonitrile in 0.10% formic acid for 8.0 min, at a flow rate of 5.0 mL min^{-1}. Upon monitoring UV absorption at 230 nm, fractions were collected by peak in 2-mL Eppendorff tubes, gently evaporated to dryness, and redissolved in deutero-methanol. NMR spectra were recorded on a 600 MHz NMR spectrometer (Model Avance AV 600, Bruker Biospin, Rheinstetten, Germany). Data extraction and analysis were carried out using OpenMS EICExtractor[18] and R.[19]

■ RESULTS AND DISCUSSION

Figure 1 illustrates the chromatograms of rapid analyses of synthetic thyroxine and its impurities both in an unstressed sample and a sample thermally stressed according to protocol 1. Besides the main peak corresponding to thyroxine, 103 and 312 masses were extracted from the chromatograms of the unstressed and thermally stressed thyroxine sample, representing 69 and 138 real impurities, respectively. In the stressed sample, the intensity of the thyroxine peak is decreased by ∼12%, as deduced from the peak areas in the ultraviolet (UV) chromatograms. Nevertheless, direct quantification with mass spectrometric detection is not possible, because of saturation of the thyroxine signal. The increase in the number and abundance of detected compounds clearly reflects the substantial impact of stressing on the number of detectable impurities.

Structural elucidation of the detected compounds was performed by using the structure of thyroxine as starting template, converting measured accurate masses into candidates for molecular formulas, and performing multistage mass spectrometry (MS^n, n = 2−6) on compounds, for which the

structure could not be unequivocally derived from the molecular formula. Finally, an extensively thermally stressed thyroxine sample (29 h at 100 °C) was subjected to micropreparative fractionation using a 150 mm × 10 mm semipreparative column, followed by analysis of the fractions by ^{1}H NMR spectroscopy, in order to confirm the suggested structures. In total, 22 of 53 different structures investigated by HRMS could be verified by NMR. The formation of 13 of the main degradation products was utilized to discuss the reaction mechanism proposed in this study. The corresponding structures, together with their MS and NMR data, are provided as Supporting Information (Table S-1).

Because of the high speed and high selectivity of the analysis method for the impurities, it was applicable to a long-term degradation study. For this experiment, a 5-g sample of thyroxine was stressed under protocol 2 under an ambient air or argon atmosphere. In order to monitor the time-dependent formation or degradation of the compounds during stressing, a total of 37 samples was taken every 15 min in the beginning and every 6 h toward the end of the stressing period and analyzed with the UHPLC-LTQ-Orbitrap-MS method, as shown in Figure 1. Figure 2 depicts representative thermal stressing profiles of 4-[4-(4-hydroxy-3,5-diiodophenyl)-tetraio-dothyronine, 3,5-diiodotyrosine, and 2-oxo-tetraiodothyroace-tamide.

From a mechanistic point of view, the kinetic plots as shown in Figure 2 allow us to draw several major conclusions about formation or degradation. First, compounds exhibiting a logarithmic decrease in concentration such as 4′-(4-hydrox-ydiiodophenyl)-tetraiodothyronine (Figure 2a) can be assumed to be already present in the unstressed compound, and they are degraded following a first-order reaction kinetics. Second, compounds that are showing a concentration increasing during the course of stressing, such as diiodothyrosine (Figure 2b), are formed either directly from thyroxine or from one of the impurities already present in the unstressed sample. Pro-nounced differences in the concentration profiles between stressing under ambient air (triangles or rectangles in Figure 2) or argon (diamonds in Figure 2) are indicative of an important role of oxygen in the degradation reaction. Finally, delayed formation of compounds, as illustrated for 2-oxo-tetraiodotyr-oacetamide in Figure 2c tells us that the compound is the product of further decomposition of a first-generation degradation product. It can be seen that oxygen concentration has a significant influence, because the delayed formation can only be recognized under limited oxygen supply as present in the closed bottle (Figure 2c, rectangles).

Utilizing the structures of the impurities derived from HRMS and NMR spectroscopy and the kinetic information as discussed above, we were able to derive a reaction scheme that can explain the formation of all major impurities and degradation products found in thermally stressed thyroxine (Figure 3). Additional information included was derived from the crystal structure of levothyroxine sodium, which crystallizes as a pentahydrate with the formula $[C_{15}H_{10}O_4NI_4]^- \cdot Na^+ \cdot 5H_2O$. In the crystal, molecules are packed through hydrophobic interactions between the aromatic rings, while the hydrophilic ends of the thyroxine molecules are connected via water-coordinated Na^+ ions and carboxyl groups, respectively, such that the lattice is formed by alternating hydrophobic and hydrophilic layers (see Figure S-2 of the Supporting Information). Thermogravimetry and powder X-ray diffrac-tometry performed by the manufacturer revealed a nearly
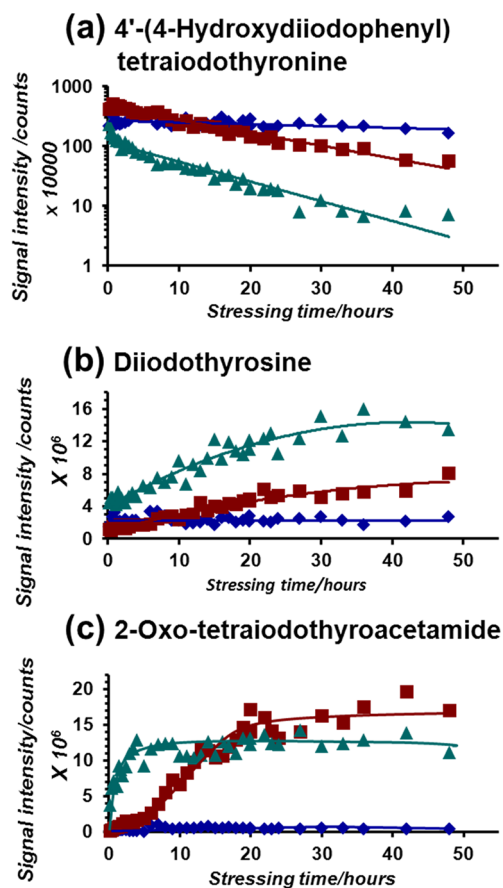

Figure 2. Thermal stressing profiles of thyroid compounds originating from (a) chemical synthesis, (b) thermal degradation, and (c) second-generation thermal degradation. Stressing profiles at 100 °C in a covered glass bottle permanently flushed with argon (diamonds), in a closed glass bottle filled with ambient air (squares), and in an open Petri dish permanently flushed with ambient air (triangles) over 48 h are shown for 4′-(4-hydroxydiiodophenyl)-tetraiodothyronine, diiodo-thyrosine, and 2-oxo-tetraiodothyroacetamide.

complete loss of crystal water and crystal integrity at 100 °C. This enhances the accessibility of the crystal for molecular oxygen and the possibility of intermolecular reactions, since, at 100 °C, (i) the side chains of thyroxine molecules are brought to spatial proximity and (ii) oxygen, as an active agent, is able to penetrate the remaining amorphous powder.

Four different bonds in thyroxine sodium salt (compound **A** in Figure 3) are eminently amenable to the initial homolytic bond breakage affected by an initiator radical such as the hydroxyl radical: the benzylic C_β−H bond in the amino acid, the phenolic O−H bond (or the O−H bond of the β-ring hydroxyl group), and the C−I bonds located at the α- or β-ring.[20−22] This was concluded from a comparison of bond dissociation energies (BDEs) of reference compounds with a similar structure (see Table 1). The high stressing temperature is assumed to enable a homolytic cleavage of the C−I bond, leading to a highly reactive phenyl radical. This most likely abstracts a hydrogen radical from a neighboring thyroxine giving triiodothyronine (**1**) as a deiodination product. The independence of this reaction pathway of the presence of oxygen is corroborated by the corresponding stressing curves that show similar slopes for all three stressing conditions (see the Supporting Information).
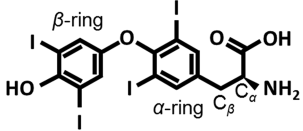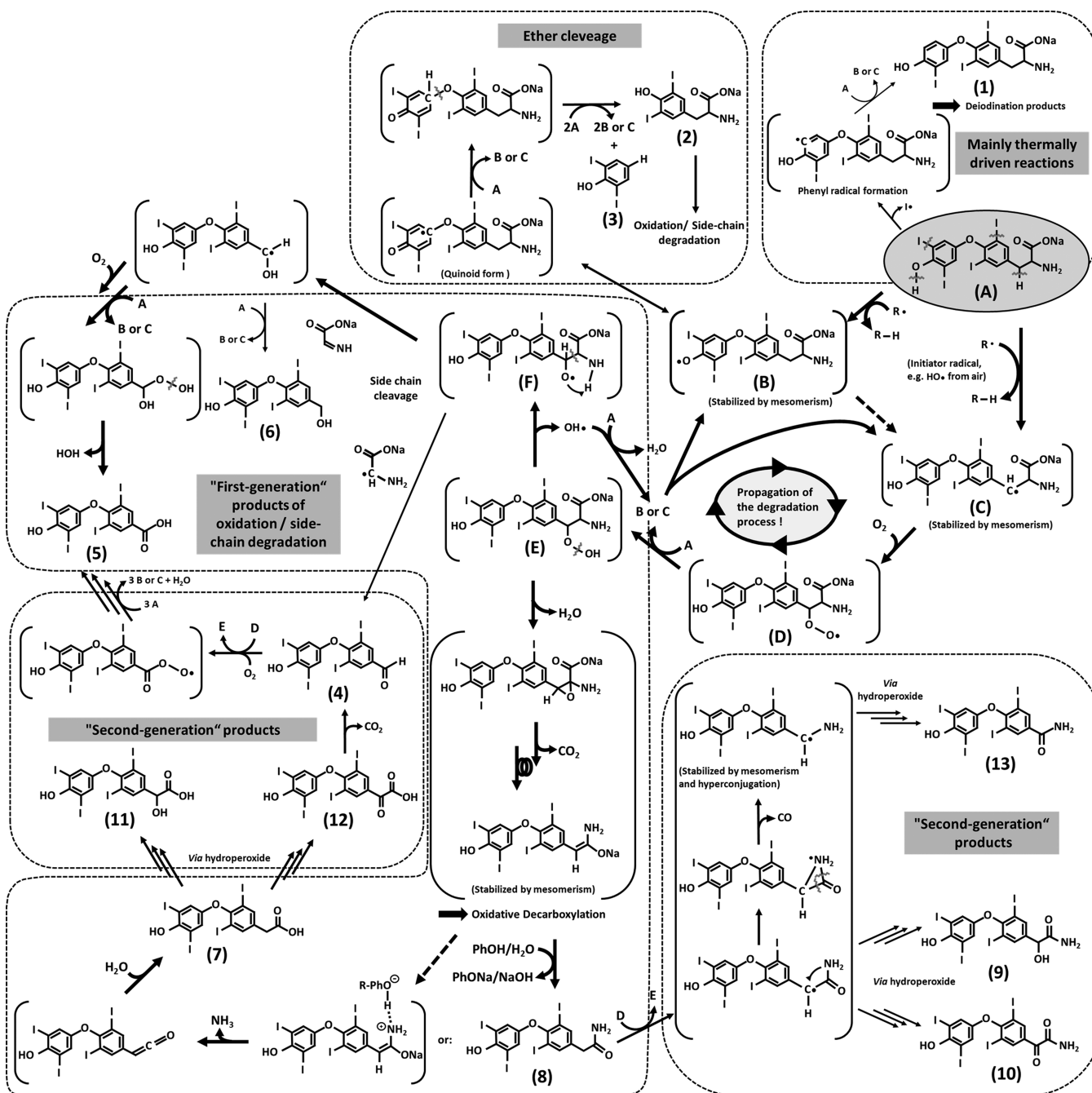
Figure 3. Proposed reaction scheme for the degradation of thyroxine under thermal stressing. The thickness of arrows represents the impact of corresponding reaction pathways within the degradation process. Stereochemistry is not taken into consideration here, although racemization and/or the formation of racemic stereocenters under the stressing conditions are likely to occur. Uppercase letters and structures shown in brackets indicate intermediates, and Arabic numerals represent end products of the degradation reactions (data sheets are available as Supporting Information).

Nevertheless, for all other reaction pathways presented here, including the propagation of the degradation process as shown in Figure 3, oxygen, as a reaction partner, plays a key role. When starting from thyroxine sodium salt as bulk material (**A**), hydrogen abstraction from the β-ring hydroxyl group or in benzylic position gives the intermediates **B** and **C**, respectively. The subsequent attack of oxygen to intermediate **C** leads to the peroxide radical **D**. The intermediate **D** is assumed to perform further hydrogen abstraction from another thyroxine molecule, giving the key intermediate **E** as well as the intermediate **C** as the starting point of a new reaction propagation cycle. The plausibility of this reaction cascade is supported by similar BDE

values for the benzylic hydrogen of thyroxine and the hydrogen of a hydroperoxide in benzyl position (377 kJ/mol vs 380 kJ/mol). This is a key feature for both an ongoing radical chain reaction and the tendency of thyroxine to form mainly side-chain degradation products under oxidative stress conditions. Alternatively, a closed reaction propagation cycle can be formulated upon the formation of the intermediate **B**, followed by a hydrogen exchange between **B** and another thyroxine (**A**), finally giving intermediate **C**. This possibility is indicated by a dashed arrow in Figure 3.

A reaction pathway designated as "ether cleavage" in Figure 3 also stands in the context of formation of intermediate **B**. By

2388

dx.doi.org/10.1021/ac303404e | Anal. Chem. 2013, 85, 2385–2390

Table 1. Bond Dissociation Energies (BDEs) Relevant for the Proposed Reaction Scheme of Thyroxine Degradation[a]

considered bond[b]	BDE [kJ/mol]	reference compound	source
Initial Bond Breakages Derived from an Intact Thyroxine Molecule			
thyroxine C_β–H	~380	tyrosine	ref 20
thyroxine β-ring O–H	~362	o-Br-phenole	ref 21, p 286
thyroxine C–I	~285	2-EtO-iodobenzene	ref 21, p 251
Radical Chain Process and Thermally Driven Reactions			
phenyl C–H	~472	benzene	ref 21, p 40
thyroxine C_β–OO radical	~92	benzyl peroxy radical	ref 21, p 340
thyroxine C_βOO–H	366–377	ROO–H	ref 21, p 268, ref 22
thyroxine C_βO–OH	180–192	RO–OH	ref 21, p 312, ref 22
HO-H	~497	water	ref 21, p 255
Side-Chain Degradation and Ether Cleavage Pathways			
thyroxine C_α–C_β	~285	benzyl methylamine	ref 21, p 198
thyroxine C_βO–H	~443	benzyl alcohol	ref 21, p 259
thyroxine C_αHN–H	~425	methylamine	ref 21, p 370
tetraiodothyro-benzaldehyde C_α–H	~347	4-PhO-benzaldehyde	ref 21, p 84

[a]Most data taken from ref 21. [b]The considered bonds for a homolytic cleavage are indicated by a hyphen between the atoms of interest. Moreover, the corresponding bond energies under standard conditions and the reference compound used for BDE estimation are given.

starting from the quinoid form of **B**, the reaction cascade is supposed to act via an entropically favored cleavage of the β-ring, followed by hydrogen abstraction from thyroxin, yielding the two molecules diiodotyrosine (**2**) and diiodophenol (**3**). The existence of such an ether cleavage pathway was supported by the degradation curves of 2,5-diiodothyrosine (**2**) and 2,5-diiodophenol (**3**) as first-generation reaction products, which show rising slopes during the thermal degradation process (see Figure 2b and the Supporting Information). Further impurities deriving from a subsequent oxidative degradation of the side chain such as 4-hydroxy-2,5-diiodobenzoic acid could be found.

Nevertheless, most of the observed reaction products are derived from oxidative degradation of the side chain starting from intermediate **E**. The labile hydroperoxide (BDE ≈ 180 kJ/mol) can undergo a homolytic cleavage, giving the hydroxyl radical and the intermediate **F** as a starting point for a side-chain cleavage reaction. Intermediate **F** undergoes either a direct C_α–C_β cleavage, giving tetraiodothyrobenzaldehyde (**4**) as a prominent impurity and a glycine radical, or an intramolecular hydrogen abstraction with concomitant C_α–C_β cleavage, leading to a mesomerism-stabilized benzyl radical as an intermediate, as well as imino glycine as a side product. Subsequently, tetraiodothyrobenzoic acid (**5**) as the main impurity and tetraiodothyrobenzylalcohol (**6**), which was found only in low amounts, can be formed upon intermolecular hydrogen abstraction directly, or after hydrogen incorporation into the reaction cascade, respectively. The degradation curve of tetraiodothyrobenzoic acid classifies this compound as a first-generation degradation product (see the Supporting Informa-

tion). An alternative formation route of tetraiodothyrobenzoic acid (**5**) via tetraiodothyroacetic acid (**7**), 2-oxo-tetraiodothyroacetic acid (**12**), and tetraiodothyrobenzaldehyde (**4**), as shown in Figure 3, is supposed to be comparably slow; therefore, it does not influence the initial course of the degradation curve.

The most remarkable reaction cascade leads to the formation of tetraiodothyroacetic acid (**7**) and tetraiodothyroacetamide (**8**) as main impurities. After intramolecular loss of water starting from intermediate **E**, oxidative decarboxylation with concomitant molecule rearrangement leads to an α-amino enolate derivative as an intermediate. The three-dimensional (3D) local environment of the enolate within the amorphous bulk material is assumed to influence the formation ratio of tetraiodothyroacetic acid and tetraiodothyroacetamide significantly. If residual crystal water is present or a phenol group is in proximity to the benzyl-position of the enolate, fast proton abstraction can occur, which facilitates the formation of tetraiodothyroacetamide (**8**). In case of an intact hydrogen bridge between the amino group of the enolate and a proximate phenol group (dashed line in Figure 3), which has been postulated to be present in crystalline thyroxine pentahydrate,[23] the elimination of ammonia becomes feasible, leading to a ketene derivative as a highly reactive intermediate. After the addition of residual crystal water or water originating from ambient air, tetraiodothyroacetic acid (**7**) is finally formed.

Regarding the mechanism of deamination as proposed by Won,[12] who postulated a cinnamic acid derivative as a product of a direct elimination of ammonia from thyroxine, we can say that such a considerably stable derivative could never be found in our study, neither in the bulk material nor at any stage of thermal stressing. Thus, we conclude that deamination in solid-state degradation does not involve direct elimination of ammonia from thyroxin by a nonradical-driven process, but rather by the proposed reaction cascades leading to the acetic acid (**7**)-, formic acid (**5**)-, benzaldehyde (**4**)-, or benzyl alcohol (**6**)-related derivatives. Interestingly, by comparing the initial phase of the degradation curves of tetraiodothyroacetic acid and tetraiodothyroacetamide, in the latter case, a slight delay until enhanced formation occurs can be observed, resulting in rather sigmoidal curve progression (see the Supporting Information). This argues for a kinetically favored reaction pathway via the ketene.

Consistently, the degradation curves of 2-hydroxy-tetraiodothyroacetamide (**9**) and 2-oxo-tetraiodothyroacetamide (**10**) as second-generation products derived from tetraiodothyroacetamide (**13**) also indicate a more distinct sigmoidal shape, compared to their analogs 2-hydroxy-tetraiodothyroacetic acid (**9**) and 2-oxo-tetraiodothyroacetic acid (**12**); see the Supporting Information). The mechanism of formation of these four impurities is analogous to the oxidation of thyroxine to its hydroperoxide (intermediate **A** to **E**), followed either by an intramolecular loss of water, giving a ketone functionality in the benzyl position, or homolytic cleavage of the hydroperoxide combined with subsequent hydrogen abstraction, giving a hydroxyl functionality.

A special case is tetraiodothyrobenzaldehyde (**4**), where the degradation curves show a rather diffuse but constant course, indicating a form of steady-state kinetics (see the Supporting Information). Because of a similar signal response under all stressing conditions, we conclude that (a) tetraiodothyrobenzaldehyde has been already present in considerable amounts in the starting material and (b) its formation and degradation during thermal stressing occurs with comparable reaction rates.

This is conclusive with the proposed formation by decomposition of 2-oxo-tetraiodothyroacetic acid (**12**), as well as the multistep auto-oxidation of tetraiodothyrobenzaldehyde (**4**) to tetraiodothyrobenzoic acid (**5**) shown in Figure 3, since both reactions are likely to be rather slow processes. The alternative route of tetraiodothyrobenzaldehyde (**4**) formation directly from intermediate **F** is supposed to play only a minor role, because of the instability of a glycine radical as a side product.

Another interesting case is the formation route of tetraiodothyrobenzamide (**13**) from tetraiodothyroacetamide (**8**). It includes the formation of an aziridine-2-one radical, which enables the entropically favored elimination of carbon monoxide. The driving force of this unusual reaction cascade is based on the additional stabilization by hyperconjugation of the shown radical intermediate having an amino group in the α position. The final reaction steps to tetraiodothyrobenzamide are supposed to act via hydroxyperoxide formation, followed by an intramolecular loss of water. In accordance with the presence of a second-generation product, the degradation curve of tetraiodothyrobenzamide describes a distinctive sigmoidal course (see the Supporting Information)

CONCLUSION

In summary, the combination of structural data from high-resolution mass spectrometry (HRMS) and nuclear magnetic resonance (NMR) spectroscopy with kinetic data obtained by means of ultrahigh-performance liquid chromatography (UHPLC) facilitated the derivation of a consistent scheme to explain all major degradation reactions and reaction products generated by the thermal stressing of thyroxine sodium salt in the solid phase. The results not only shed light on the radical-driven solid–phase degradation reactions effective in drug decomposition but also help to characterize the origin of impurities detectable in unstressed thyroxine. Because thermal and oxidative reactions, as well as radical reactions that are initiated by UV irradiation, can be assumed to be the major limitation of stability of solid drugs, our workflow offers a generic approach to study compound decomposition in the solid state, as enforced by international guidelines for conducting stability testing of drug substances.[24]

ASSOCIATED CONTENT

Ⓢ Supporting Information

This material is available free of charge via the Internet at http://pubs.acs.org.

AUTHOR INFORMATION

Corresponding Author

*Tel.: (+)43 662 8044 5738. Fax: (+)43 662 8044 5751. E-mail: c.huber@sbg.ac.at. Homepage: www.uni-salzburg.at/molbiol/chemie.

Notes

The authors declare no competing financial interest.

ACKNOWLEDGMENTS

REFERENCES

(1) Committee for Medicinal Products for Human Use. *Guideline on Safety and Efficacy Follow-Up Risk Management of Advanced Therapy Medicinal Products*; European Medicines Agency: London, 2008.

(2) Zhang, J. S.; Lazar, M. A. *Annu. Rev. Physiol.* **2000**, *62*, 439−466.

(3) Soldin, O. P.; Soldin, S. J. *Clin. Biochem.* **2011**, *44*, 89−94.

(4) Escobar-Morreale, H. F.; Botella-Carretero, J. I.; Escobar del Rey, F.; Morreale de Escobar, G. *J. Clin. Endocrinol. Metab.* **2005**, *90*, 4946−4954.

(5) Kendall, E. C. *J. Biol. Chem.* **1919**, *39*, 125−147.

(6) Harington, C. R.; Barger, G. *Biochem. J.* **1927**, *21*, 169−183.

(7) Chalmers, J. R.; Dickson, G. T.; Elks, J.; Hems, B. A. *J. Chem. Soc.* **1949**, 3424−3433.

(8) Salamonczyk, G. M.; Oza, V. B.; Sih, C. J. *Tetrahedron Lett.* **1997**, *38*, 6965−6968.

(9) Andre, M.; Domanig, R.; Riemer, E.; Moser, H.; Groeppelin, A. *J. Chromatogr. A* **1996**, *725*, 287−294.

(10) Gostomski, I.; Braun, R.; Huber, C. G. *Anal. Bioanal. Chem.* **2008**, *391*, 279−288.

(11) Gika, H.; Lämmerhofer, M.; Papadoyannis, I.; Lindner, W. *J. Chromatogr. B* **2004**, *800*, 193−201.

(12) Won, C. M. *Pharm. Res.* **1992**, *9*, 131−137.

(13) MacNair, J. E.; Lewis, K. C.; Jorgenson, J. W. *Anal. Chem.* **1997**, *69*, 983−989.

(14) Hu, Q.; Noll, R. J.; Li, H.; Makarov, A.; Hardman, M.; Graham Cooks, R. *J. Mass Spectrom.* **2005**, *40*, 430−443.

(15) Pan, C. K.; Liu, F.; Ji, Q.; Wang, W.; Drinkwater, D.; Vivilecchia, R. *J. Pharm. Biomed. Anal.* **2006**, *40*, 581−590.

(16) Pilaniya, K.; Chandrawanshi, H. K.; Pilaniya, U.; Manchandani, P.; Jain, P.; Singh, N. *J. Adv. Pharm. Technol. Res.* **2010**, *1*, 302−310.

(17) Zhu, D. A.; Zhang, G. G.; George, K. L.; Zhou, D. *J. Pharm. Sci.* **2011**, *100*, 3529−3538.

(18) Sturm, M.; Bertsch, A.; Gropl, C.; Hildebrandt, A.; Hussong, R.; Lange, E.; Pfeifer, N.; Schulz-Trieglaff, O.; Zerck, A.; Reinert, K.; Kohlbacher, O. *BMC Bioinf.* **2008**, *9*, 163.

(19) R Development Core team. *R: A Language and Environment for Statistical Computing*, 2008, http://www.r-project.org, accessed Sept. 18, 2009.

(20) Ly, T.; Julian, R. R. *J. Am. Chem. Soc.* **2008**, *130*, 351−358.

(21) Luo, Y.-R., Ed. *Comprehensive Handbook of Chemical Bond Energies*; CRC Press: Boca Raton, FL, 2007.

(22) Schoneich, C.; Hovorka, S. W. *J. Pharm. Sci.* **2001**, *90*, 253−269.

(23) Katrusiak, A. *J. Pharm. Sci.* **2004**, *93*, 3066−3075.

(24) International Conference on Harmonisation of Technical Requirements for Registration of Pharmaceuticals for Human Use. *ICH Topic Q 1 A (R2), Stability Testing of New Drug Substances and Products*; European Medicines Agency: London, 2003.